

# Numerical Investigation on the Mechanism of Double-Volute Balancing Radial Hydraulic Force on the Centrifugal Pump

## **Authors:**

Ye Yuan, Shouqi Yuan, Lingdi Tang

*Date Submitted:* 2019-12-09

*Keywords:* transient pressure variation, steady pressure distribution, radial hydraulic force, double-volute, centrifugal pump

## *Abstract:*

Double-volute is an effective technique to reduce radial hydraulic force on the centrifugal pump and thereby mitigate the pump-casing vibration induced by unsteady flow characteristics. The mechanism of the double-volute structure balancing radial force on the impeller and volute was investigated on the basis of volute cross-sections by using Computational Fluid Dynamics (CFD) method. The tested performances and simulated inner-flow characteristics of two pumps with single-volute and double-volute were compared in this paper. The performance-test results verify the veracity of CFD method and illustrate that double-volute pump has some losses in terms of pump head and operation efficiency. The numerical simulations reveal that double-volute pump has smaller radial-force magnitude than single-volute pump on the abnormal conditions. Steady pressure field and transient pressure variations of pumps were explored to account for radial-force characteristics of double-volute pump. Compared with the single-volute structure, obvious pressure increases were found in the upper chamber (single part) of the double-volute, while the static pressure decreased in the lower chamber (double chambers). This situation reduces the pressure difference between two volute cross-sections in the collinear radial direction, resulting in smaller radial hydraulic force. Moreover, the transient simulations present the same phenomenon. The radial-forces distribute more uniformly in the double-volute pump, which can alleviate some vibrations.

*Record Type:* Published Article

*Submitted To:* LAPSE (Living Archive for Process Systems Engineering)

*Citation (overall record, always the latest version):*

LAPSE:2019.1280

*Citation (this specific file, latest version):*

LAPSE:2019.1280-1

*Citation (this specific file, this version):*

LAPSE:2019.1280-1v1

*DOI of Published Version:* <https://doi.org/10.3390/pr7100689>

*License:* Creative Commons Attribution 4.0 International (CC BY 4.0)

Article

# Numerical Investigation on the Mechanism of Double-Volute Balancing Radial Hydraulic Force on the Centrifugal Pump

Ye Yuan \*, Shouqi Yuan and Lingdi Tang

Research Center of Fluid Machinery Engineering and Technology, Jiangsu University, Zhenjiang 212013, China; shouqiy@ujs.edu.cn (S.Y.); angelattld@163.com (L.T.)

\* Correspondence: sfri\_yy@126.com

Received: 29 August 2019; Accepted: 29 September 2019; Published: 2 October 2019



**Abstract:** Double-volute is an effective technique to reduce radial hydraulic force on the centrifugal pump and thereby mitigate the pump-casing vibration induced by unsteady flow characteristics. The mechanism of the double-volute structure balancing radial force on the impeller and volute was investigated on the basis of volute cross-sections by using Computational Fluid Dynamics (CFD) method. The tested performances and simulated inner-flow characteristics of two pumps with single-volute and double-volute were compared in this paper. The performance-test results verify the veracity of CFD method and illustrate that double-volute pump has some losses in terms of pump head and operation efficiency. The numerical simulations reveal that double-volute pump has smaller radial-force magnitude than single-volute pump on the abnormal conditions. Steady pressure field and transient pressure variations of pumps were explored to account for radial-force characteristics of double-volute pump. Compared with the single-volute structure, obvious pressure increases were found in the upper chamber (single part) of the double-volute, while the static pressure decreased in the lower chamber (double chambers). This situation reduces the pressure difference between two volute cross-sections in the collinear radial direction, resulting in smaller radial hydraulic force. Moreover, the transient simulations present the same phenomenon. The radial-forces distribute more uniformly in the double-volute pump, which can alleviate some vibrations.

**Keywords:** centrifugal pump; double-volute; radial hydraulic force; steady pressure distribution; transient pressure variation

## 1. Introduction

Centrifugal pump has extensively applied to many industries closely related with people's work and life, such as aviation, auto industry, petrochemical industry, and so on. The pump can provide fluid with high head and large flow, especially in terms of conveying corrosive fluid. For the large centrifugal pump, the radial force has been proven to affect the stability of pump operation. Specifically, the pump shaft and the sealing ring are damaged mainly by large radial force on the impeller. These forces are induced by some nonuniform flows in the pump. In recent years, double-volute is an effective means to the design of centrifugal pump, which cannot only inherit advantages of single-volute pump, but also effectively decreases the radial hydraulic force generating in the flow field of pump because of pump operation and asymmetric structure of volute [1,2].

Most research focused on the characteristics of radial force and the hydraulic performances of double-volute pump [3–5]. Empirical correlation and experimental method were the main tools of studying force characteristics by measuring and predicting force magnitude in the twentieth century. Based on impeller geometry, pump head, flow-rate conditions and the effect of pump specific speed on

radial forces, some force models were proposed for the calculation of radial forces [6,7]. Comparing with the predictions of the correlation, static force measurements have been made, and radial-force characteristics on the impeller and volute were investigated [8–10]. These published results revealed that the double-volute had the positive effect on decreasing the radial hydraulic force on the centrifugal pump at the off-design conditions.

Over the past few decades, with the rapid development in computer, Computational Fluid Dynamics (CFD) has been widely applied in studying and solving some problems occurred in pump design and operation. The effects of pump geometric parameters on the radial hydraulic force and flow characteristics in the pump with double-volute have been investigated by CFD model [11–13]. The impeller-volute interaction is the main reason causing some unsteady forces on the impeller due to pressure pulsations and the momentum exchange between impeller and volute [14]. The existence of volute tongue especially results in large difference of static pressure distributions between both sides of the tongue, which induces obvious hydraulic force along the radial direction from impeller to volute [15,16]. Meanwhile, geometric parameters of division plate placed in the single-volute for cutting apart the volute chamber into two chambers have been proven to be crucial to volute performances and radial force [17,18].

Despite a set number of literatures documenting radial-force characteristics and pump performance of double-volute pump, there are few detailed investigations into the key factor resulting in the decrease of this hydraulic force. Two volute schemes of single-volute and double-volute are designed on the basis of volute cross-sections in order to investigate steady and unsteady flow characteristics in the double-volute pump for studying the effects of double-volute on the radial hydraulic force. CFD method is used to simulate steady pressure field and transient pressure variations in the pump, and its veracity is verified by pump performance test.

## 2. Materials and Methods

### 2.1. Pump Specifications

The model pump considered in the paper is the centrifugal pump with the rotating speed of 2900 r/min. The pump head ( $H$ ) and nominal flow rate ( $Q_N$ ) are 18 m and 30 m<sup>3</sup>/h respectively. Its main geometric characteristics are summarized in Table 1. The pump impeller has six blades, while the volute has two schemes of single-volute structure and double-volute structure, as shown in Figure 1. The volutes are built from the volute cross-sections situated in the critical positions where the flow parameters are directly exposed in Figure 2 and Table 2. The choices of these positions were dictated by industry-recognized design experience and previous studies [19,20]. The metal plate dividing into one volute chamber into two sections, starts at volute cross-section 4 and ends at section 9 in the double-volute structure. This plate has the thickness of 4 mm. The area ratios of volute chambers of pumps with single-volute and double-volute are provided in Figure 3 for comparison. The area ratio  $A$  was defined as  $A = S_1:S_0$ , thereinto  $S_1$  is the area of volute cross-section, and  $S_0$  is the area of impeller outlet. The single-volute structure is spiral in form while the double-volute structure is divided into the forequarter of a single volute and the combination of the single-volute forequarter and the fifth cross-section of the single volute. However, the area ratios of these two volutes are close for ensuring the similar flow areas of the volutes.

**Table 1.** Geometric characteristics of model pump.

impeller inlet diameter, $d_1/m$	0.065
impeller outlet diameter, $d_2/m$	0.13
impeller outlet width, $b/m$	0.0095
base volute diameter, $d_3/m$	0.14
outlet flange diameter, $d_4/m$	0.05

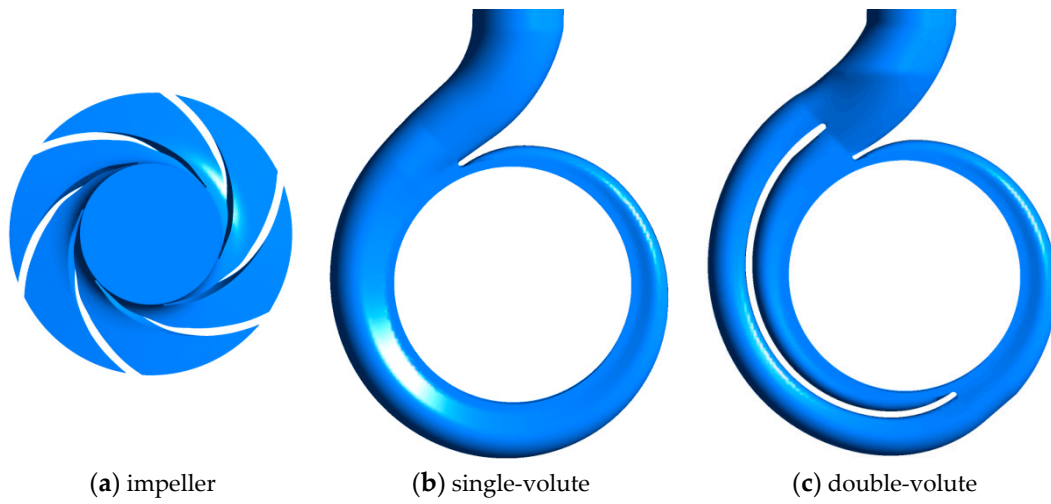


Figure 1. Model pump.

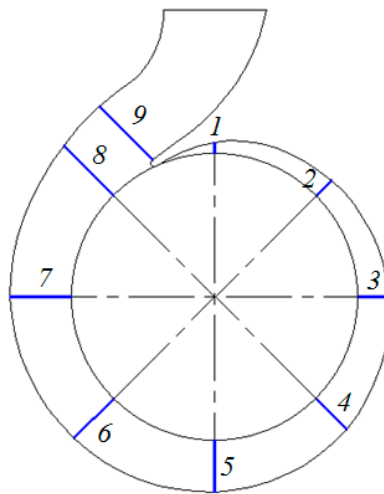


Figure 2. Cross-sections of volute.

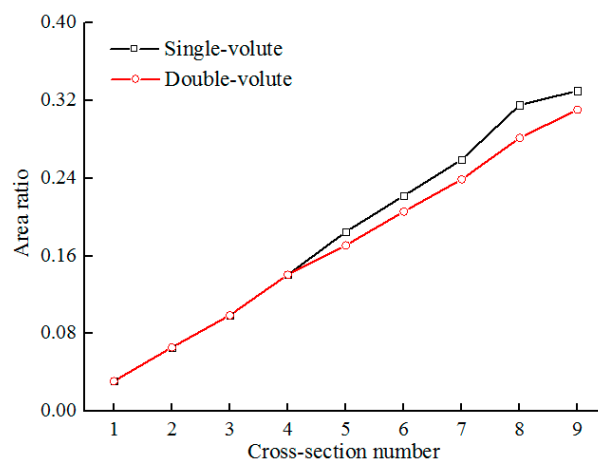
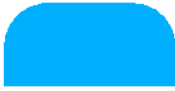






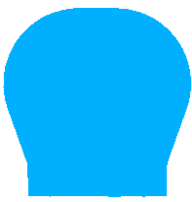
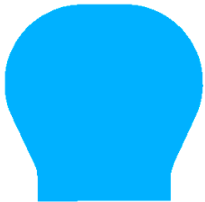

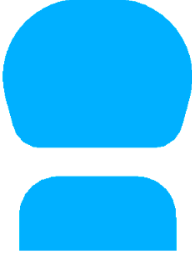
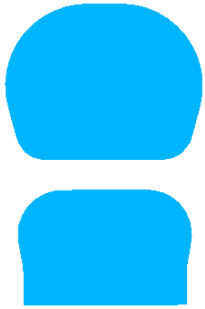
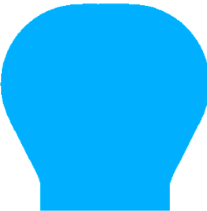
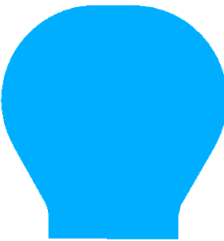
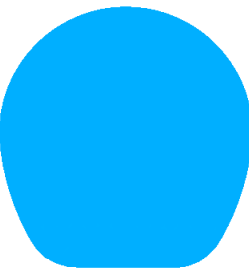
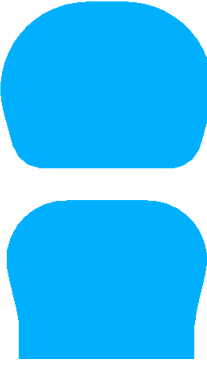
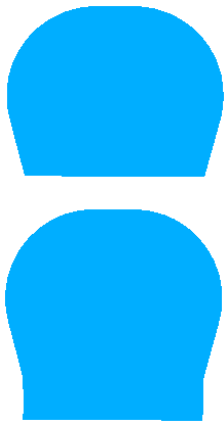
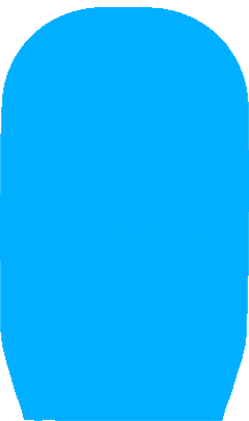


Figure 3. Area ratios.

**Table 2.** Volute cross-section shape.

Cross-section	1	2	3
single-volute			
double-volute			
Cross-section	4	5	6
single-volute			
double-volute			
Cross-section	7	8	9
single-volute			
double-volute			

## 2.2. Experimental Measurements

The test rig of pump performance characteristics was built and the performance test for the model pumps with single-volute and double-volute were conducted to study the effect of double-volute structure on the pump performance. The numerical model used in the paper was also verified by experimental data. Figure 4 shows the testing apparatus, including a tested pump, two pressure sensors, an electromagnetic flowmeter, pipeline, some regulating valves, and a data acquisition system. The tested pump installed on test platform is presented in Figure 5. The test facilities and measurement techniques are adequate to the specific requirements [21]. The water at the 25° was used for the working fluid in the experiment.

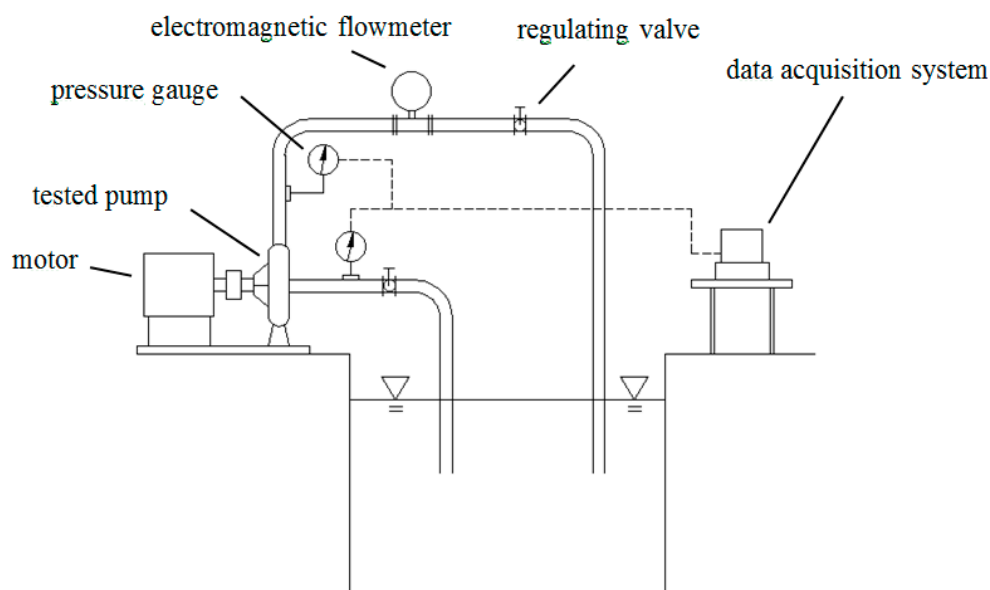


Figure 4. Schematic diagram of experimental apparatus.



Figure 5. Tested pump.

The uncertainty analysis of the test was conducted before measuring the pump performance. The test uncertainty  $e$  is composed of random uncertainty  $e_R$  and system uncertainty  $e_S$ .

$$e = \sqrt{e_R^2 + e_S^2} \quad (1)$$

For the  $e_R$ , the mathematic average  $\bar{x}$  of the observation  $x_i (i = 1, 2, \dots, n)$  is calculated by the following formula. The observation  $x_i$  represents pump head  $H$ , flow rate  $Q$  or pump efficiency  $\eta$ .

$$\bar{x} = \frac{1}{n} \sum x_i \quad (2)$$

where  $n$  is the reading number.

The standard deviation  $s$  of this set of observations is

$$s = \sqrt{\frac{1}{n-1} \sum (x_i - \bar{x})^2} \quad (3)$$

The uncertainty  $e_R$  induced by random effect is

$$e_R = \frac{100ts}{\bar{x}\sqrt{n}} \% \quad (4)$$

when the reading number  $n$  is six times, the value  $t$  is 2.57.

The system uncertainty  $e_S$  is determined by the measuring instrument accuracy. The electromagnetic flowmeter with the accuracy  $\pm 0.3\%$  was used for measuring the pump flow rate. The pump inlet and outlet pressure were measured by pressure sensors with the uncertainty of  $\pm 0.25\%$ . The impeller speed and the rotation shaft torque were also measured by the torque speed sensor with the accuracy  $\pm 0.2\%$ .

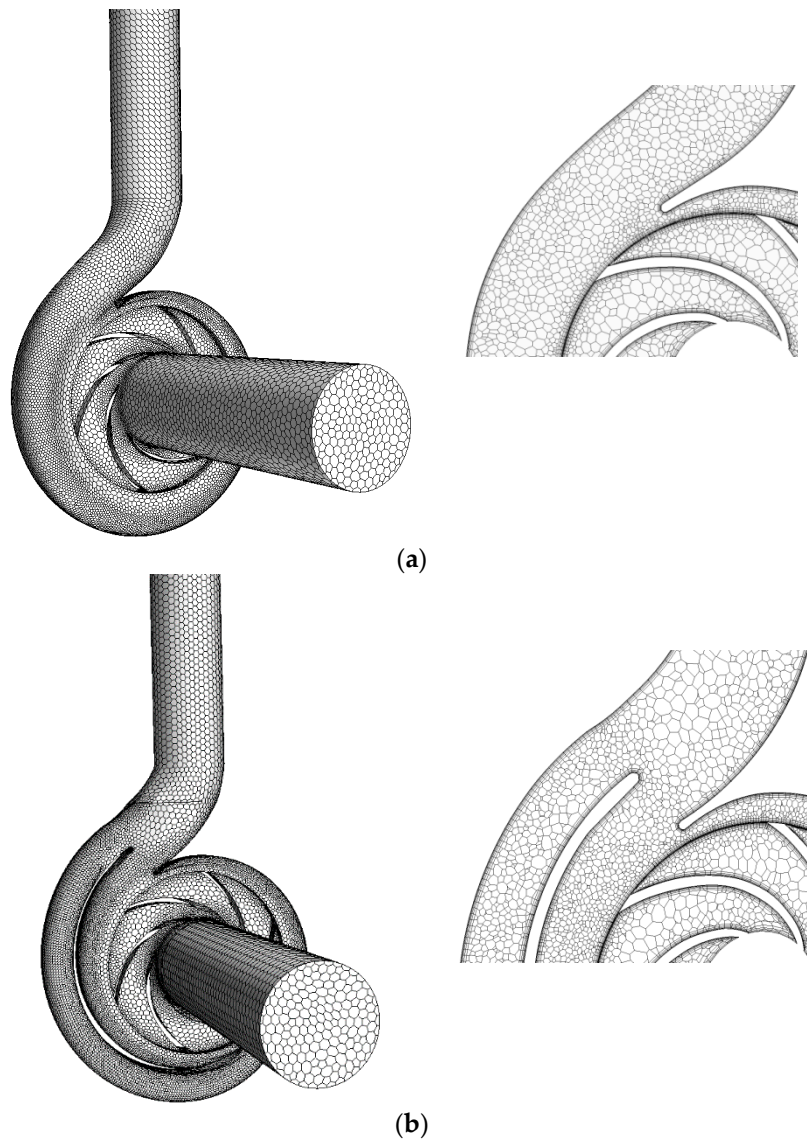
Based on above calculations, the uncertainties of pump head, flow rate, and pump efficiency are shown in Table 3.

**Table 3.** Measurement uncertainty.

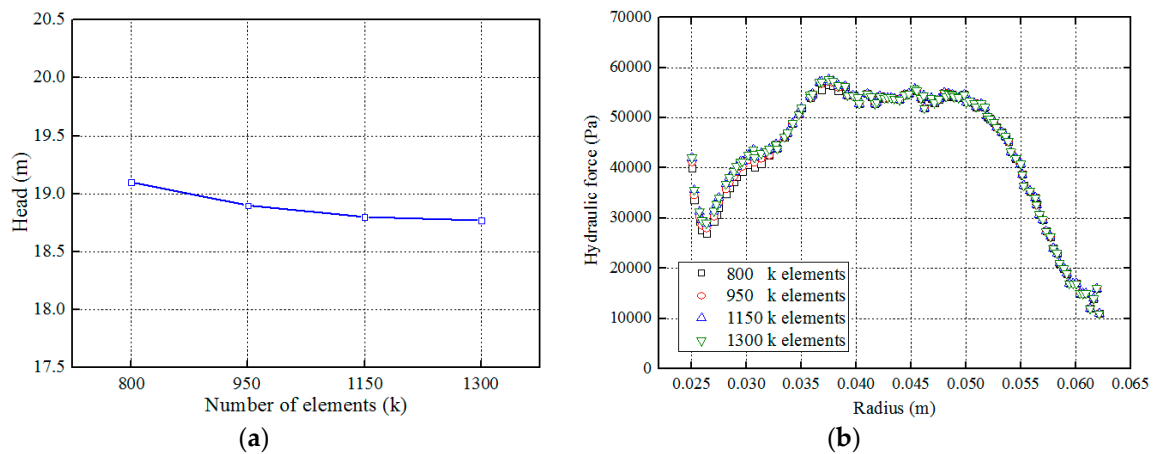
Performance Characteristics	Pump Head	Flow Rate	Pump Efficiency
Uncertainty (%)	$\pm 0.82$	$\pm 1.18$	$\pm 1.26$

### 2.3. CFD Methodology

Steady pressure field and transient pressure variations in the model pump with the impeller rotating were studied, and the effects of double-volute structure on characteristics of radial hydraulic force were analyzed. For the numerical simulation, computing domains of pumps with single-volute structure and double-volute structure were created, and Figure 6 shows two domains including the inlet duct, impeller, volute, and the outlet duct. The polyhedral mesh was generated for each independent domain and the mesh density was also studied to verify the mesh independent for the simulated solution. The head and hydraulic force on the blade of single-volute pump were selected as the variables of reference to analyze the mesh independence. Figure 7a presents that the simulated value of pump head tends to be stable after the mesh element number reaches 1.15 million. Some hydraulic forces on one blade are generated because of pressure differences between blade suction side and blade pressure side. These forces have been shown in Figure 7b and distribute steadily when the mesh element number exceeds 0.95 million. Therefore, considering the significant computational saving, the mesh with 1.15 million elements was used for present simulations. The maximum nondimensional wall distance  $y^+$  values of single-volute pump domain and double-volute pump domain were less than 85 and 90, respectively, which could satisfy the requirement of the turbulence modeling method used in this paper.



**Figure 6.** CFD domain meshes. Close-up view into the volute and impeller: (a) pump with the single-volute structure (b) pump with double-volute structure.



**Figure 7.** Mesh independence analysis: pump head and hydraulic force on the blade at the design condition based on four mesh numbers: (a) pump head (b) hydraulic force on the blade.



Steady and unsteady flows were numerically simulated to study pump performance and flow characteristics in the pump by the general software ANSYS FLUENT. The same computational domains were used in steady and unsteady simulations. The results of the steady simulations were used as the initial conditions for the unsteady ones. 3D Reynolds averaged Navier-Stokes equations have been considered. The mass conservation equation and momentum conservation equation can be written as:

$$\frac{\partial}{\partial x_i}(\rho u_i) = 0 \quad (5)$$

$$\frac{\partial}{\partial x_j}(\rho u_i u_j) = -\frac{\partial p}{\partial x_i} + \frac{\partial}{\partial x_j} \left[ \mu \left( \frac{\partial u_i}{\partial x_j} + \frac{\partial u_j}{\partial x_i} \right) \right] + \frac{\partial}{\partial x_j} (-\rho \overline{u_i' u_j'}) + F_i \quad (6)$$

where  $\rho$  is liquid density,  $\mu$  is dynamic viscosity and  $F_i$  is source item.

The Shear Stress Transport (SST) turbulence model [22] was used for enclosing the equations. This model is a hybrid model of  $k - \omega$  and  $k - \epsilon$  turbulence models, which can switch automatically in between near-wall area and main flow area. The transport equations for  $k$  and  $\omega$  are as follows:

$$\frac{\partial}{\partial t}(\rho k) + \frac{\partial}{\partial x_i}(\rho u_i k) = \tilde{P}_k - \beta^* \rho k \omega + \frac{\partial}{\partial x_i} \left[ (\mu + \sigma_k \mu_t) \frac{\partial k}{\partial x_i} \right] \quad (7)$$

$$\frac{\partial}{\partial t}(\rho \omega) + \frac{\partial}{\partial x_i}(\rho u_i \omega) = \alpha \frac{1}{v_t} \tilde{P}_k - \beta \rho \omega^2 + \frac{\partial}{\partial x_i} \left[ (\mu + \sigma_\omega \mu_t) \frac{\partial \omega}{\partial x_i} \right] + 2(1 - F_1) \rho \sigma_{\omega 2} \frac{1}{\omega} \frac{\partial k}{\partial x_i} \frac{\partial \omega}{\partial x_i} \quad (8)$$

$$v_t = \frac{a_1 k}{\max(a_1 \omega, SF_2)} \quad (9)$$

$$S = \sqrt{2S_{ij}S_{ij}} \quad (10)$$

$$P_k = \mu_t \frac{\partial u_i}{\partial x_j} \left( \frac{\partial u_i}{\partial x_j} + \frac{\partial u_j}{\partial x_i} \right) \rightarrow \tilde{P}_k = \min(P_k, 10 \cdot \beta^* \rho k \omega) \quad (11)$$

$$F_1 = \tanh \left\{ \left\{ \min \left[ \max \left( \frac{\sqrt{k}}{\beta^* \omega y'}, \frac{500v}{y^2 \omega} \right), \frac{4\rho \sigma_{\omega 2} k}{CD_{k\omega} y^2} \right] \right\}^4 \right\} \quad (12)$$

$$F_2 = \tanh \left\{ \left[ \max \left( 2 \frac{\sqrt{k}}{\beta^* \omega y'}, \frac{500v}{y^2 \omega} \right) \right]^2 \right\} \quad (13)$$

$$CD_{k\omega} = \max \left( 2\rho \sigma_{\omega 2} \frac{1}{\omega} \frac{\partial k}{\partial x_i} \frac{\partial \omega}{\partial x_i}, 10^{-10} \right) \quad (14)$$

where the coefficients are as follows:  $\beta^* = 0.09$ ,  $\alpha_1 = 5/9$ ,  $\beta_1 = 0.075$ ,  $\sigma_{k1} = 0.85$ ,  $\sigma_{\omega 1} = 0.5$ ,  $\alpha_2 = 0.44$ ,  $\beta_2 = 0.0828$ ,  $\sigma_{k2} = 1.0$ ,  $\sigma_{\omega 2} = 0.856$ .

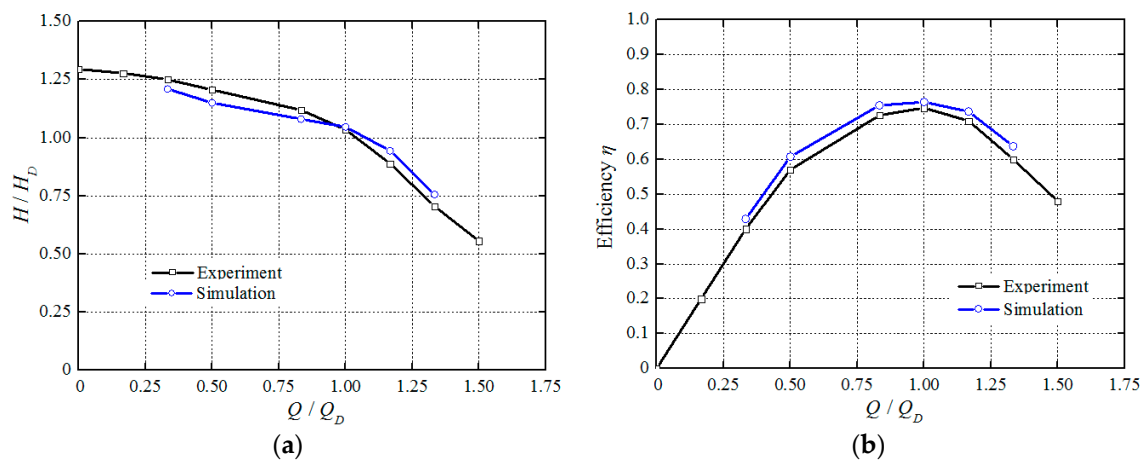
The impeller is defined as the rotational component, while the inlet duct, volute, and the outlet duct are considered under stationary. The Frozen Rotor interface was used in the connection interface between pump impeller and volute. Table 4 presents the boundary conditions used in the numerical simulations.

**Table 4.** Boundary conditions used in the numerical simulation.

Location	Boundary Condition	Option
Inlet duct	Inlet	Velocity
Outlet duct	Outlet	Mass flow rate
Solid surfaces	Wall	No slip wall

In the unsteady simulations, the discretization in space was of second-order accuracy, and the discretization in time used second-order backward Euler scheme. The Frozen Rotor interface in the steady simulations become the transient rotor–stator. Moreover, the convergence criteria for all variables were set as  $10^{-5}$ . The revolution of three degree was set as the time step, and eight revolutions of the impeller rotation was chosen as the duration time.

Furthermore, the numerical model used in the paper was verified by comparing with the pump performance tested in the experiment. Figure 8 shows simulated pump performance curves as well as the tested characteristic curves. From the head and operating efficiency curves of the single-volute pump, the agreement between the simulated results and the experimental data was observed. The maximum errors for pump head and operating efficiency are 6.64% and 6.73%, respectively, and the error of the simulated pump performance on the normal condition is the minimum.



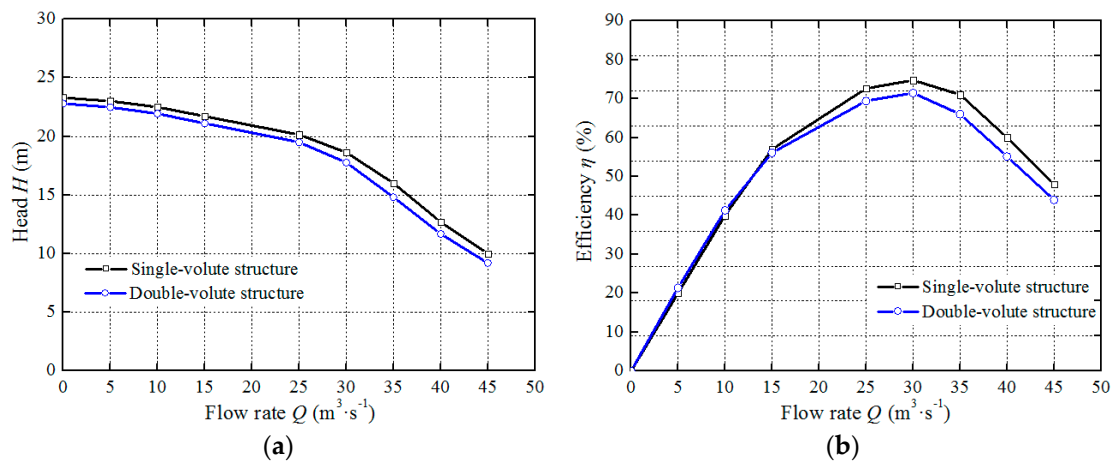
**Figure 8.** Comparison of experimental and numerical results: (a) head curve (b) efficiency curve.

### 3. Results and Discussions

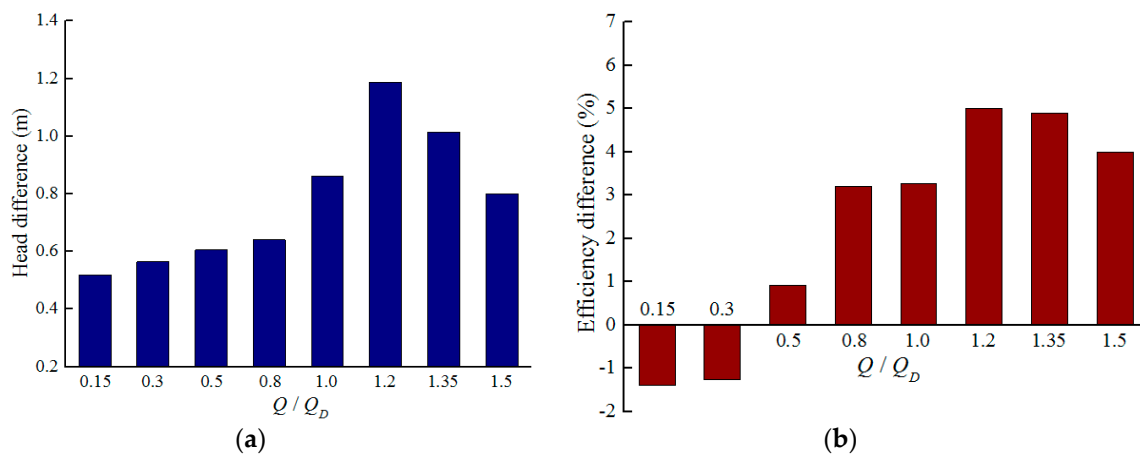
#### 3.1. Pump Performance

##### 3.1.1. Comparison of Test Performance Characteristics

Performance characteristics of pumps with single-volute and double-volute were tested, and tested results in comparison are presented in Figure 9. The head values of single-volute pump and double-volute pump at the rated flow are 18.9 m and 18.1 m, respectively, reaching the design requirement (18 m). Despite the decrease in pump efficiency, the double-volute model is still an effective technique applied in the engineering. Single-volute pump has a little higher head than double-volute pump in the whole flow range. This head difference gradually increases when the flow rate goes up to  $35 \text{ m}^3/\text{h}$  from pump startup, as shown in Figure 10. The maximum difference is about 1.2 m when the flow rate reaches  $35 \text{ m}^3/\text{h}$ . The head difference on the large-flow condition is obviously higher than that of the low-flow condition. Meanwhile, operation efficiencies of pumps encounter similar situation. The efficiency of single-volute pump is higher than that of double-volute pump on the large-flow condition. The maximum difference between pump efficiencies is about 5% when the flow rate increases to  $35 \text{ m}^3/\text{h}$ . Tested performance results illustrate that the double-volute structure has a big effect on pump performance on the large-flow condition, both pump head and operation efficiency decline obviously.



**Figure 9.** Performance characteristics of pumps with the single-volute structure and the double-volute structure: (a) head curve (b) efficiency curve.



**Figure 10.** Difference values of performance characteristics: (a) pump head (b) operation efficiency.

### 3.1.2. Comparison of Radial Hydraulic Forces on Pumps

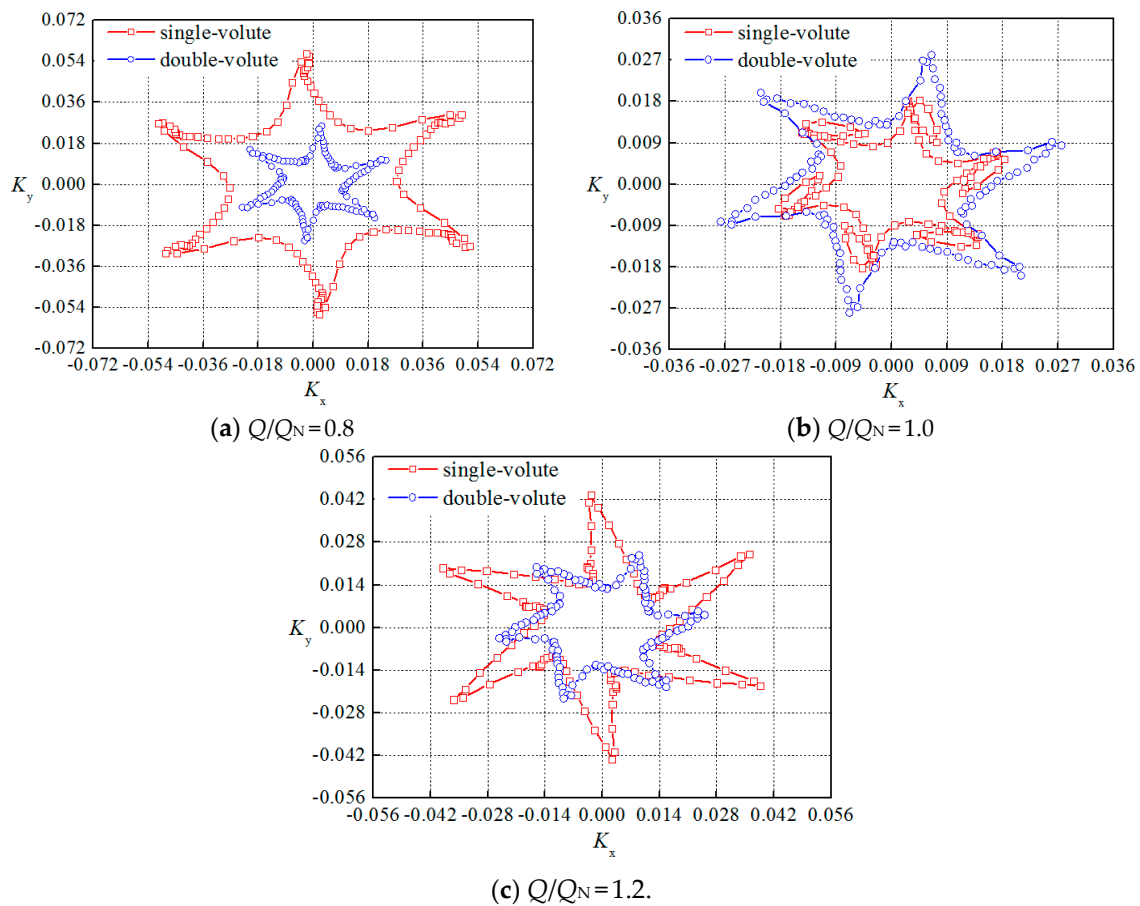
The vector of radial hydraulic force on the pump can be decomposed into two orthogonal component forces,  $F_x$  and  $F_y$ , which are lay on the radial section of pump. The force vector orientation is referenced from the first cross-section of volute in the rotating coordinate direction, and positive in the direction of impeller rotation. The force is normalized by the force coefficient  $K$  based on the impeller outlet tip velocity:

$$K = \frac{20F}{\pi \rho D b u^2} \quad (15)$$

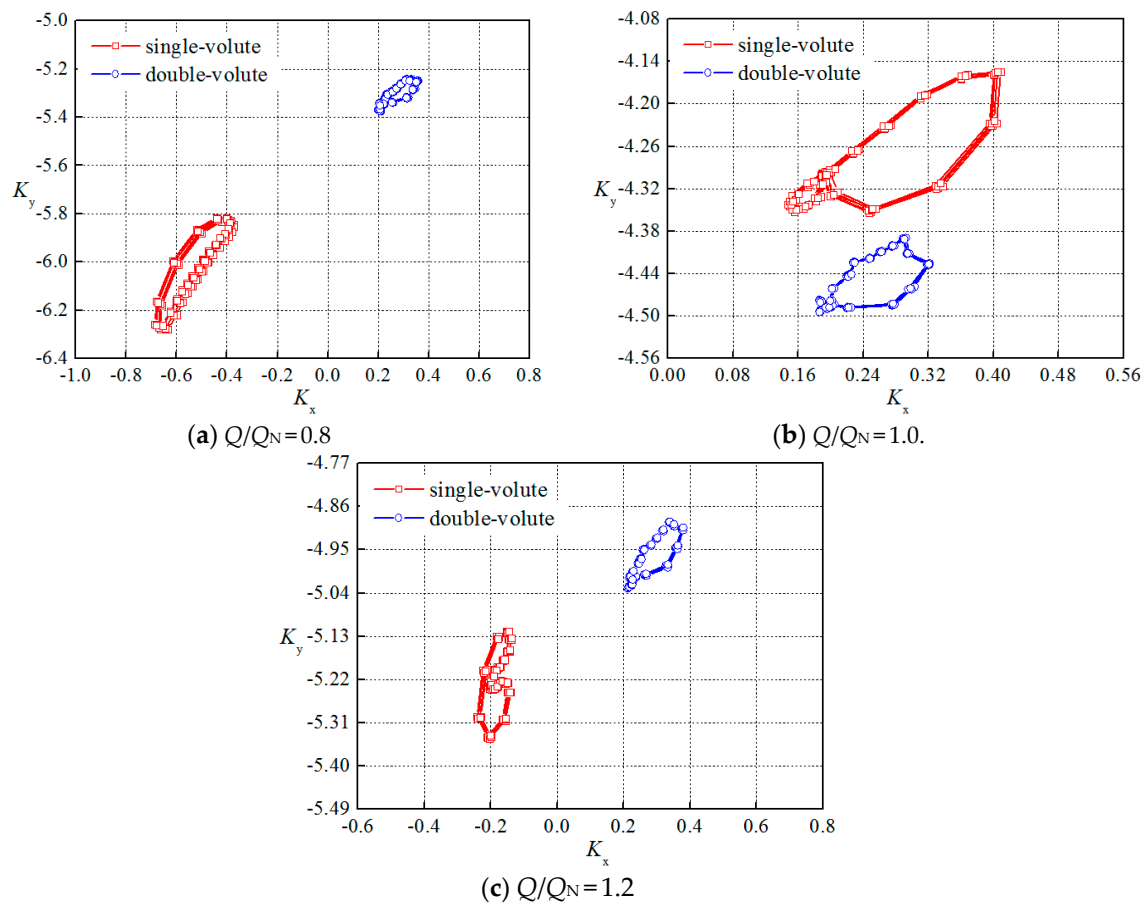
where  $F$  is the radial hydraulic force (N),  $D$  is the impeller diameter (m),  $b$  is the impeller width (m), and  $u$  is the circumferential velocity in the largest base circle of the impeller (m/s).

The radial hydraulic forces on the impeller and volute within one cycle of impeller rotation for different flow rates ( $0.8Q_N$ ,  $Q_N$  and  $1.2Q_N$ ) are shown in Figures 11 and 12 using the force coefficient. Radial hydraulic forces on the impeller regularly develop and revolve around the origin in the coordinate system. The variations of these forces are exhibited in obvious periodicity, affected by impeller structure because of blade number. The force pulsations excite the pump casing to vibrations [20]. The fluid flows from the rotating impeller uniformly and impacts on the asymmetric structure of the volute. The impeller-volute interference produces some radial hydraulic forces. The bigger the pulsation amplitude is, the more severely the pump vibrates. On the normal condition of  $Q_N$ , radial hydraulic force on the pump with single-volute is apparently smaller than that on the

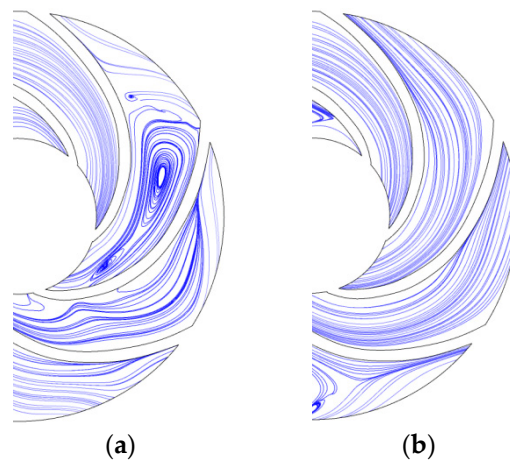
double-volute pump. However, bigger force on the pump with single-volute arises at  $0.8Q_N$  and  $1.2Q_N$ , which illustrates positive effects of double-volute on the force pulsation variation for abnormal conditions. The existence of second volute tongue is in favor of homogeneous flows in the pump because of the double-volute structure superior to the asymmetric structure of the single volute. As shown in Figure 13, some unsteady flows developing severely on abnormal conditions can be improved, such as flow recirculation and stall. These simulated force characteristics and unsteady flows correspond to published literatures [8–10]. Smaller force amplitude contributes to mitigating the pump-casing vibration, and then makes the pump run more reliably. Meanwhile, these forces on the volute are trapped in the fourth quadrant, which indicates the direction of pump-case vibration inducing by radial hydraulic force.



**Figure 11.** Radial hydraulic forces on the impeller.



**Figure 12.** Radial hydraulic forces on the volute.



**Figure 13.** Unsteady flows in impeller passages at  $0.8Q_N$ : (a) single-volute pump (b) double-volute pump.

### 3.2. Steady-State Pressure Field

Because of asymmetric structure of pump volute, pressure difference in flow field is generated between both cross-sections (seen in Figure 2) in the collinear radial direction, such as volute cross-sections 1–5, 2–6, 3–7, or 4–8. This pressure difference can induce radial hydraulic force acting upon impeller or volute.

Figure 14 shows pressure contours at the mean rotational planes of pumps with single-volute and double-volute for different flow rates ( $0.8Q_N$ ,  $Q_N$  and  $1.2Q_N$ ). From the impeller inlet to the

volute outlet, the pressure energies of water gradually increase in both pumps. The working fluids flowing from impeller to volute are well homogeneous for two pumps. However, along volute cross-sections 1–8, there is a trend of water pressure increasing in the flow field which verifies the generation of radial hydraulic force. Moreover, some flow disturbances are observed around blade tip and volute tongue, due to wake flow in the outlet of blade passage and flow impact on the tongue. Obviously, the area of this flow-disturbance region in double-volute pump is bigger than that in single-volute pump. This change of the flow can affect flow structure in the pump and then cause the hydraulic force variation. This phenomenon is caused by the interaction between the blade tip and the second volute tongue.

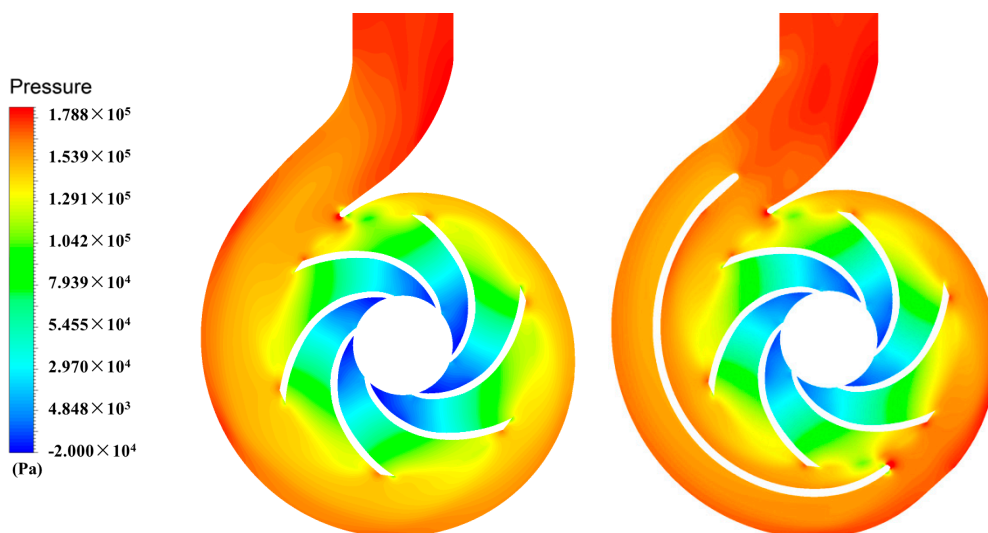
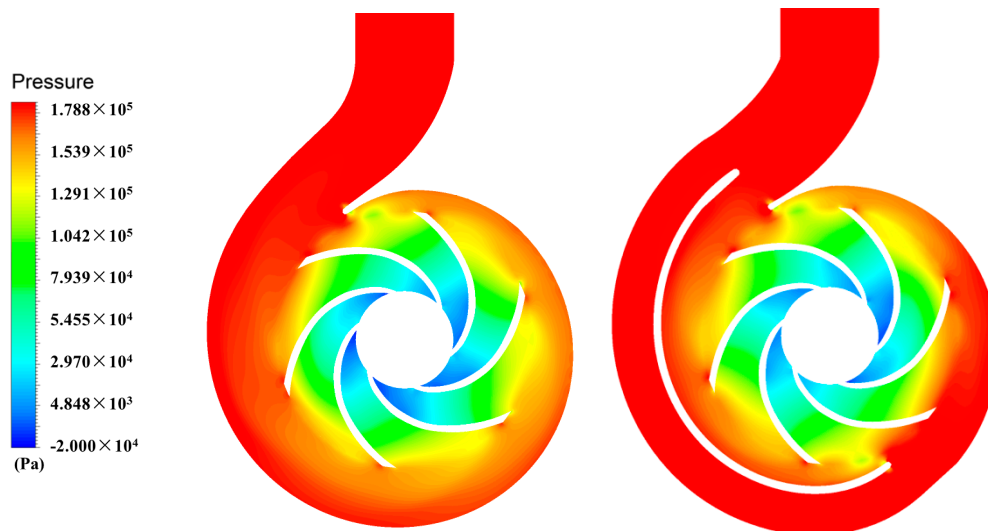
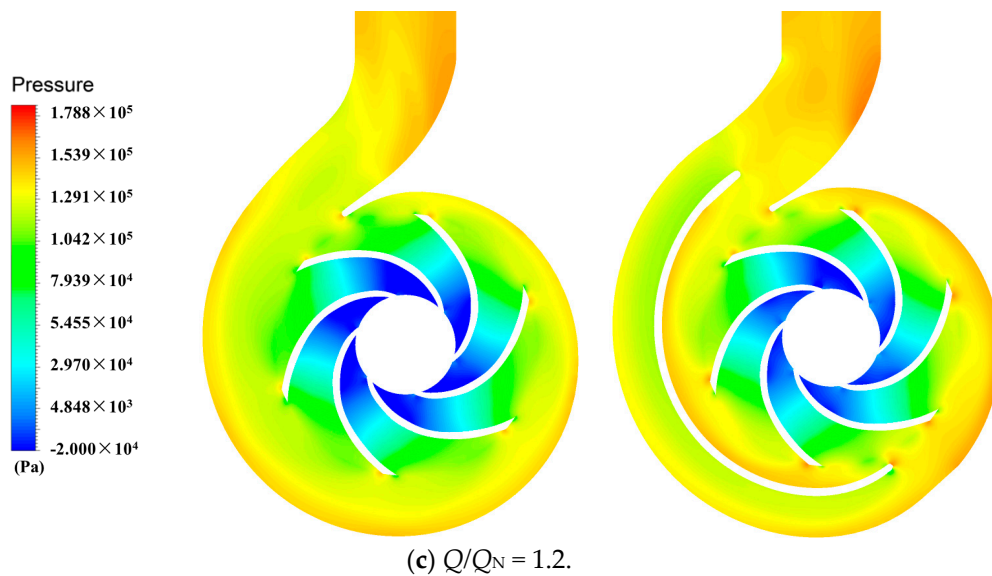


Figure 14. Cont.



**Figure 14.** Steady-state pressure distributions in the radial cross-sections.

The isolation plate of double-volute can cause some friction loss, which induces that the pump works at the rated flow with small decline. This phenomenon results in a few drops in the pressure field of impeller inlet. However, considering both head curves and internal pressure fields of these two pumps, this pressure drop has less effects on the pump performance and cavitation.

For different operation conditions in Figure 14, comparisons of inner flow characteristics in the pumps with single-volute and double-volute are close, so the normal flow rate was selected as the research subject for exploring pressure distributions in the volute cross-sections in Figure 15. The water distributes high pressure to low pressure from top to bottom in the section, which shows that the high pressure region locates at the outside surface of the volute-chamber inner wall. For the double-volute, the difference between downside pressure and upside pressure of the plate produces some energy expenditure due to the existence of the metal plate. This could ultimately lead to the decreasing of pump efficiency and radial hydraulic force.

Meanwhile, these two volutes have the same shape and size for cross-sections 1–4, but higher pressure exists in the flow field of the pump with double-volute. The double-volute facilitates the fluid energy transformation from kinetic energy to pressure energy. After the fourth section, an annular volute was separated from the spiral passage in the double-volute. The high pressure fluid flows past the annular volute according to pressure contours in the cross-sections 5–8. The high pressure energy is concentrated in the upper volute separated from the tongue, while the fluid energy transformation in the under volute is not sufficient due to the comparatively shortened volute passage. Therefore, the fluid entering the volute passage with the double-volute carries a large portion of unconverted kinetic energy, which results in a considerable amount of friction loss and various hydraulic losses. This explains that the head and operation efficiency of double-volute pump is lower than that of the single-volute pump. Moreover, the integration between the increase of pressure energy in cross-sections 1–4 and the loss of kinetic energy in cross-sections 5–8 may cause the decrease of pressure difference in flow field along the radial direction, which takes positive effect of balancing radial hydraulic force.

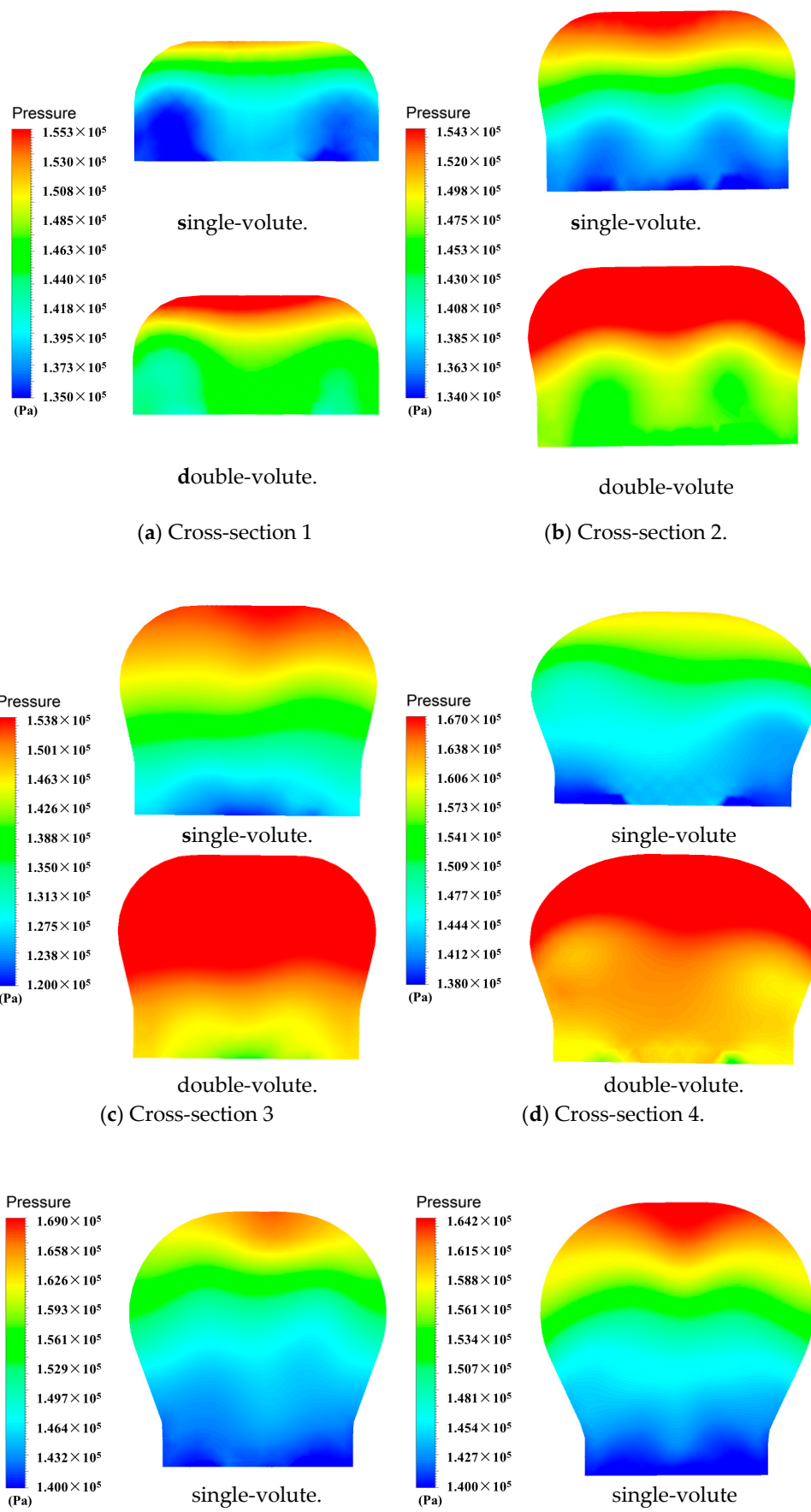


Figure 15. Cont.



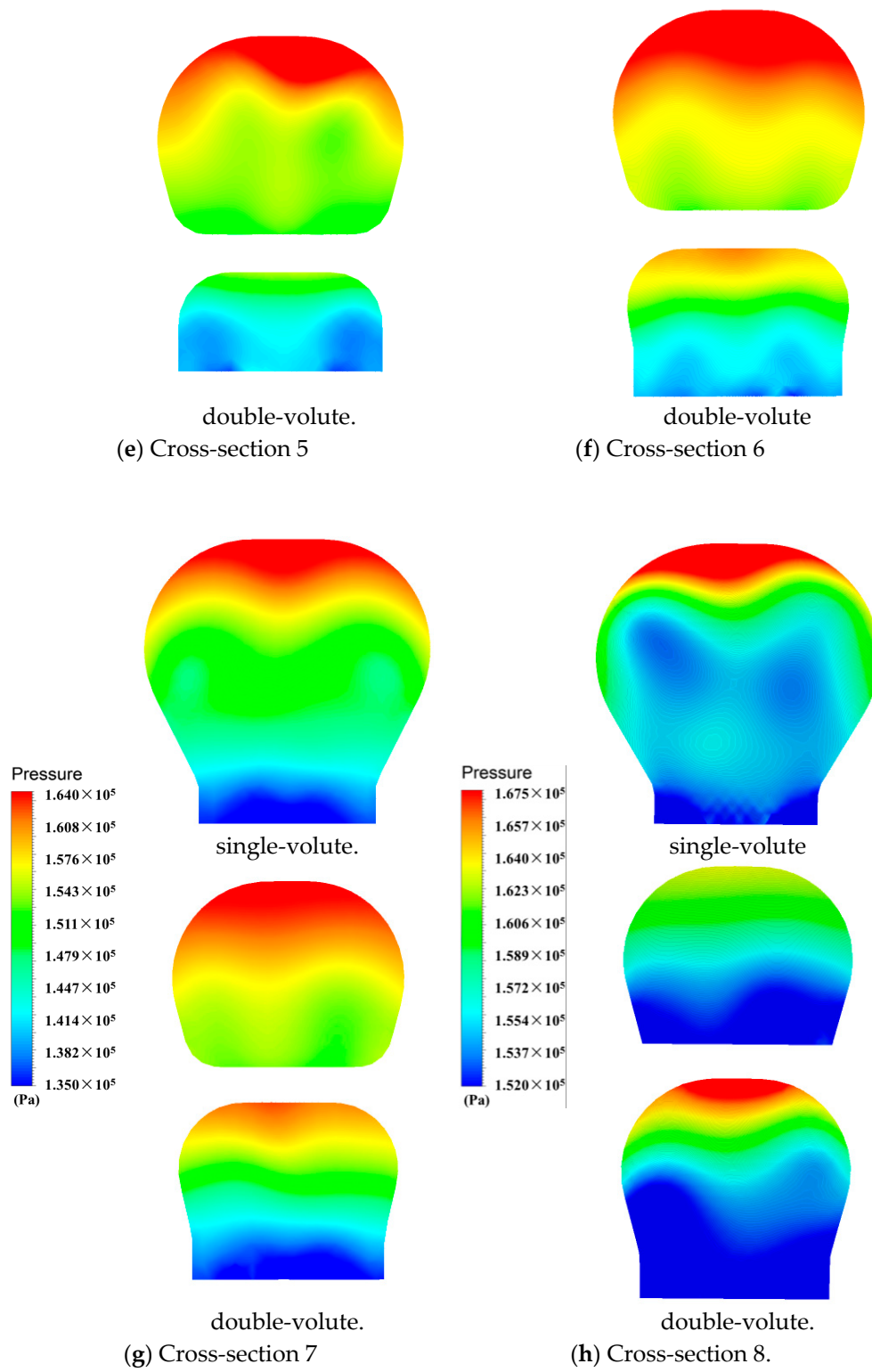
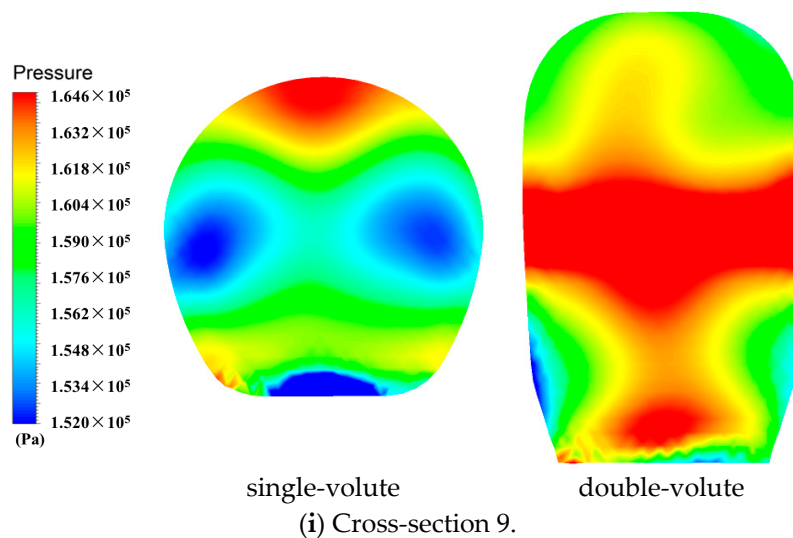


Figure 15. Cont.



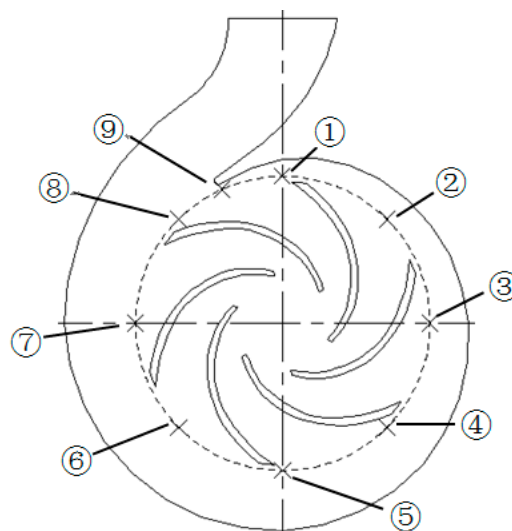
**Figure 15.** Steady-state pressure distributions in the volute cross-sections.

### 3.3. Transient Pressure Variations

Steady-state analysis for pressure field preliminarily indicates the reason of double-volute balancing hydraulic force. This section reveals transient pressure variations in the pumps with single-volute and double-volute on the basis of recorded data by monitoring points arranged in the flow channel. Figure 16 shows the positions of monitoring points located in a circle with the diameter of 0.135 m. These points were evenly distributed in the base circle and corresponded to volute sections. Meanwhile, the static pressure is normalized by the pressure coefficient  $C$  using a dynamic pressure based on the impeller outlet tip velocity:

$$C = \frac{\Delta p}{\frac{1}{2}\rho u^2} \quad (16)$$

where  $\Delta p$  was used for evaluating the periodic pressure and depended on the unsteady pressure  $p$  at a grid node and the time-averaged pressure  $\bar{p}$ , defined as  $\Delta p = p - \bar{p}$ . The standard deviation of the normalized unsteady pressure was calculated by the dynamic pressure based on the impeller tip speed  $u$ . The water density  $\rho$  is 997.05 kg/m<sup>3</sup> at the 25 degrees centigrade.



**Figure 16.** Monitoring point locations.

The monitored pressures experience periodical variation with impeller rotating in one full cycle as shown in Figure 17, and it is demonstrated that the variation period depends on the impeller structure with a certain number of blades. For the monitoring points 1–4, the pressure magnitudes of double-volute pump are obviously higher than that of single-volute pump, which is in line with steady-state pressure distributions in the volute cross-sections. The water from the volute chamber with the region from volute cross-sections 1–4 in the single-volute pump, can interact with the tongue and converting kinetic energy into pressure energy when flows to section 9. Nevertheless, this energy transformation in the double-volute pump happens in advance when the water flows past cross-section 4. This situation causes that the double-volute has the higher-pressure magnitude. For the monitoring points 5–8, the pressure nearly develops in the double-volute pump along the track of the pressure variation in the single-volute pump, but has the slightly high amplitude. Figure 17 presents transient pressure variations in the two pumps for the rated flow rate  $Q_N$ , and similar periodical variations occur in the pressure fields for the low flow rate  $0.8Q_N$  and the large flow rate  $1.2Q_N$ , except for different magnitudes in the pressure developing processes for different conditions.

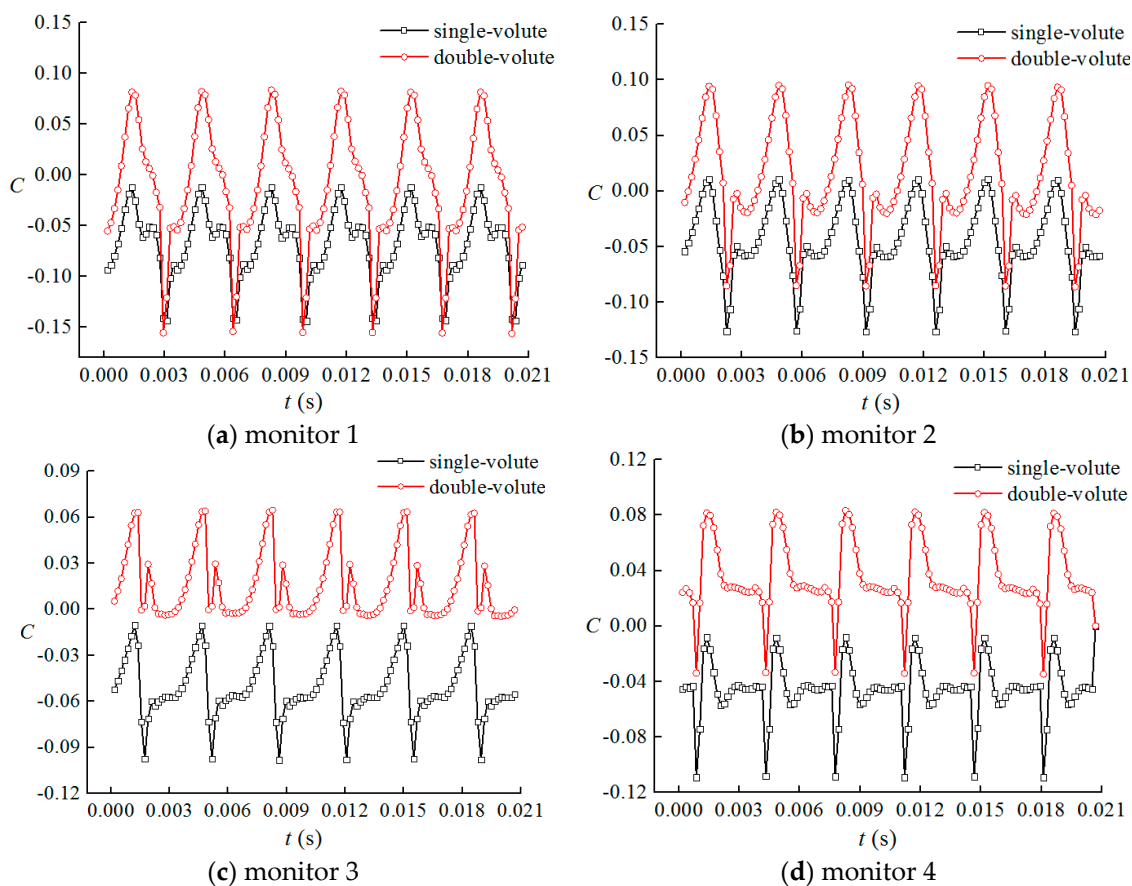


Figure 17. Cont.

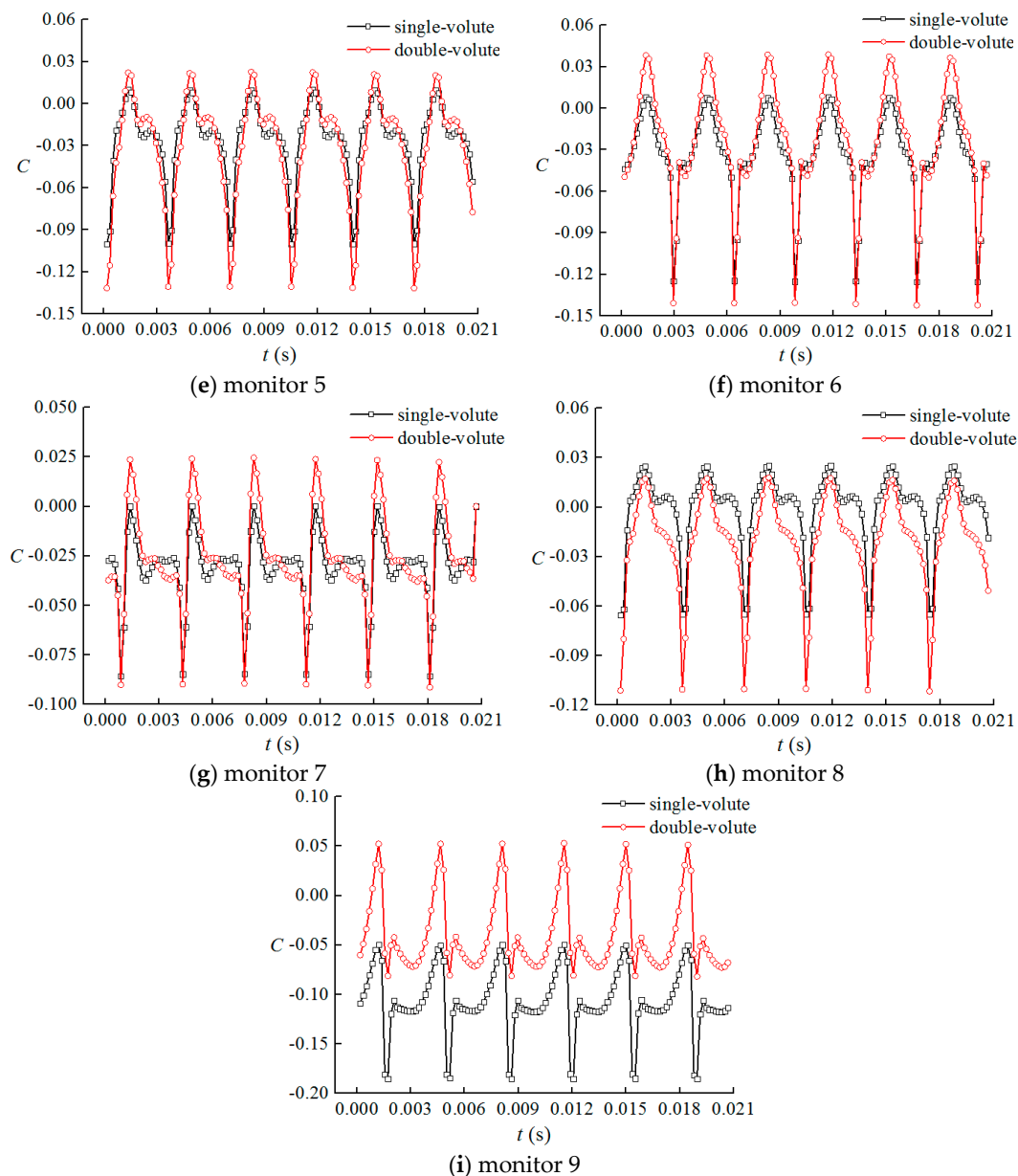


Figure 17. Monitored pressure variations.

For exploring the comparison of pressure variations in the flow fields of both pumps, contrast pressures at the initial moment and the maximum by comparing single-volute pump with double-volute pump are presented in Figures 18 and 19. While pressures at the monitoring points 1–4 of double-volute pump have large increment in comparison to that of single-volute pump, pressures in the double-volute cross-sections 5–8 have the decrement or small increment. This circumstance of pressure distributions in both pumps indicates that the hydraulic force in the radial direction of double-volute pump is smaller than that of single-volute pump, which is verified by comparison of pressure differences between collinear sections of both pumps in Figures 20 and 21. Both initial pressure difference and maximum pressure difference illustrate that smaller pressure difference exists in the single-volute pump for normal condition (seen in Figures 20b and 21b), while the opposite circumstance is presented for abnormal conditions. These pressure differences for different conditions coincide with characteristics of radial hydraulic forces on the pumps with single-volute and double-volute investigated in the Section 3.1.2, which is thus seen as a reason of generating radial hydraulic forces.

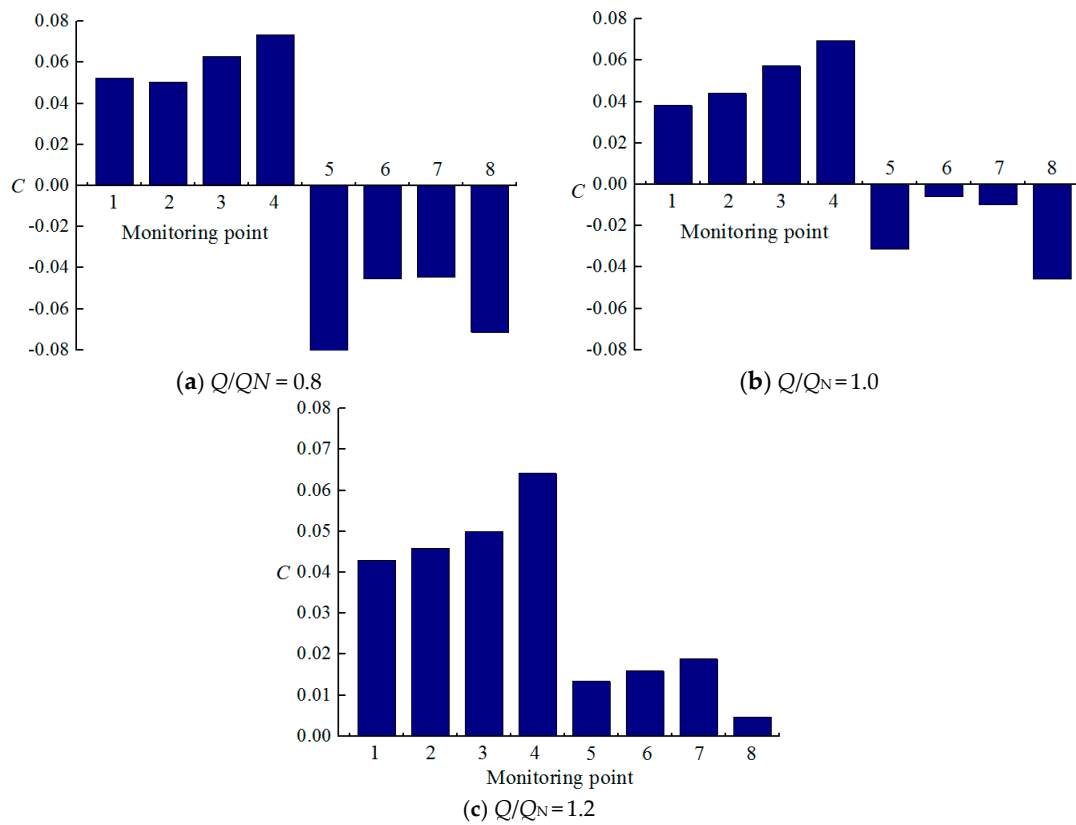


Figure 18. Monitored initial pressure variations from single-volute pump to double-volute pump.

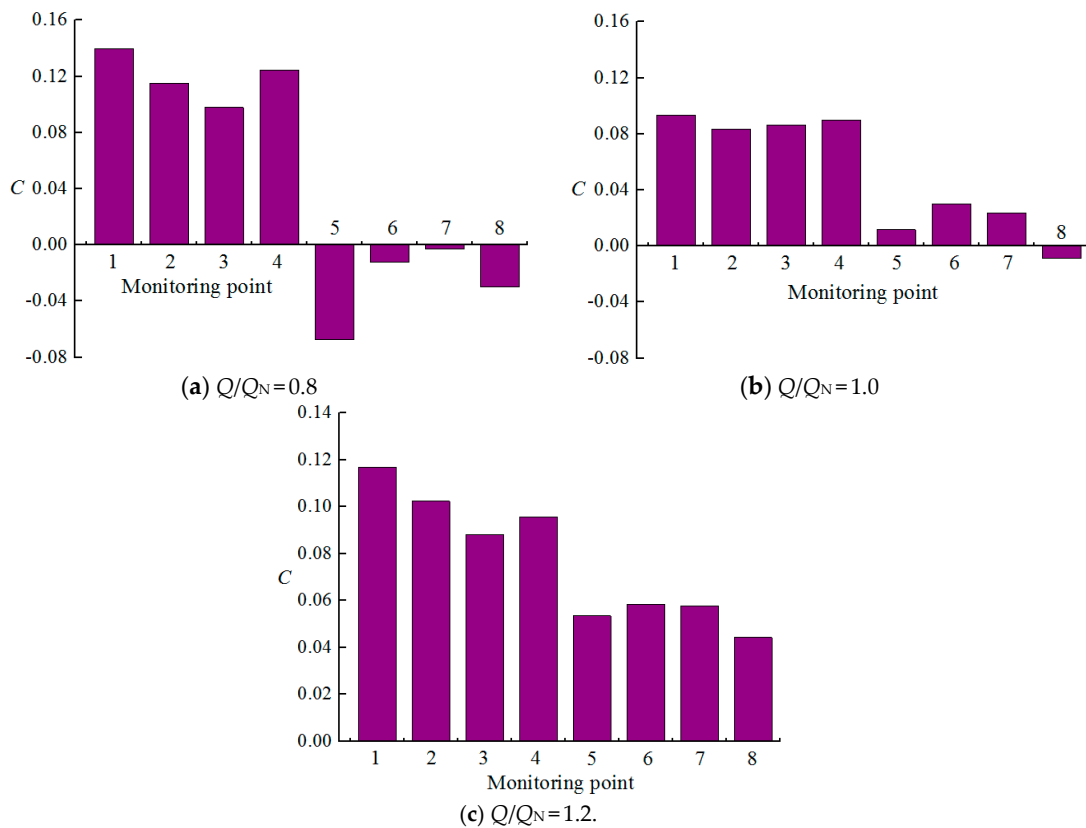


Figure 19. Monitored maximum pressure variations from single-volute pump to double-volute pump.

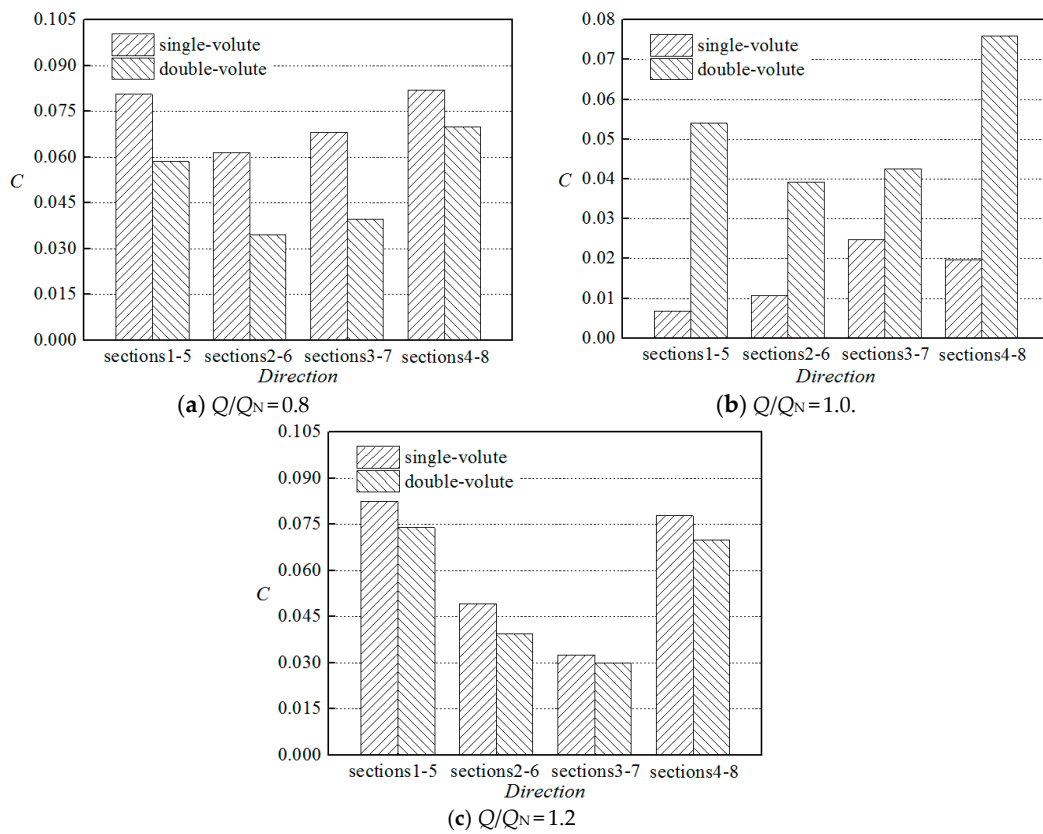


Figure 20. Initial pressure difference between collinear sections.

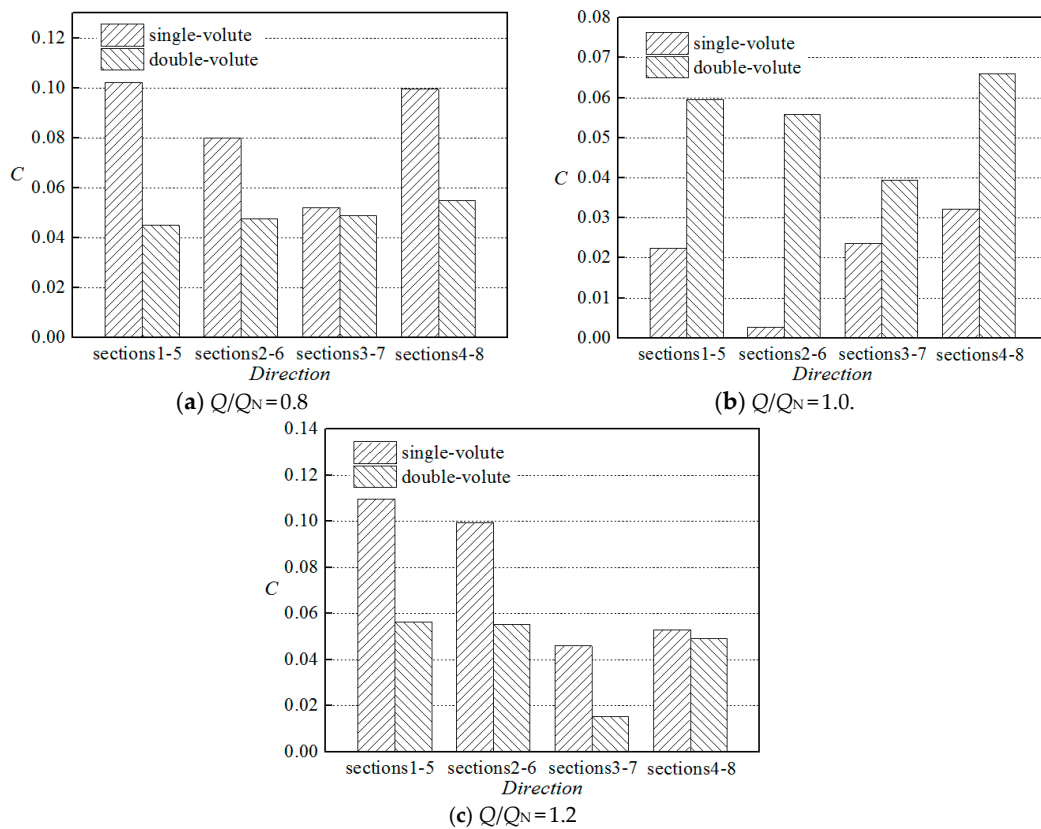


Figure 21. Maximum pressure difference between collinear sections.

#### 4. Conclusions

The tested performances and simulated radial-force characteristics of two pumps with single-volute and double-volute were compared in this paper. Two volute schemes were designed on the basis of volute cross-sections situated in the critical positions. The performance-test results verify the veracity of CFD method used to study the mechanism of double-volute structure balancing radial hydraulic force on impeller and volute and illustrate that the double-volute structure has a small negative effect on pump head and operation efficiency. The numerical simulations reveal that double-volute pump has smaller radial-force magnitude than single-volute pump on the abnormal conditions, which corresponds to published literatures. Steady pressure field and transient pressure variations of pumps were explored to account for radial-force characteristics of double-volute pump based on volute cross-sections. Obvious pressure increases were found in steady pressure fields of cross-sections 1–4 of double-volute, which decrease the pressure difference between two sections in the collinear radial direction. Meanwhile, based on transient pressure variations with the impeller rotating, pressure-fluctuate amplitudes in the cross-sections 1–4 present significant increase, while that in the cross-sections 5–8 show decrease or modest increase. This situation results in smaller pressure difference existed in the double-volute pump along the radial direction, which coincides with radial-force characteristics. Therefore, the pressure field changed by double-volute structure is an evident reason of decreasing radial hydraulic force on centrifugal pump.

**Author Contributions:** Supervision, S.Y.; Writing—original draft preparation, Y.Y.; Writing—review and editing, Y.Y.; Simulated and analyzed data, L.T.

**Funding:** This research is sponsored by the Natural Science Foundation of Jiangsu Province of China for Young Scholars (Grant No. BK20180876), the Natural Science Foundation of China (Grant No. 51779107), the Industry-College-Institute Cooperation Project of Jiangsu Province of China (Grant No. BY2018027) and the China Postdoctoral Science Foundation (Grant No. 2019M651735).

**Conflicts of Interest:** The authors declare that they do not have any commercial or associative interests that represent a conflict of interests in connection with the work.

#### References

1. Lobanoff, V.S.; Ross, R.R. *Centrifugal Pumps: Design & Application*; Gulf Publishing Company: Houston, TX, USA, 1992.
2. Xiao, R.F.; Lü, T.F.; Wang, F.J. Influence of rib structure in double-volute centrifugal pumps on the impeller radial force. *Trans. Chin. Soc. Agric. Mach.* **2011**, *42*, 85–88.
3. Spence, R.; Amaral-Teixeira, J. A CFD parametric study of geometrical variations on the pressure pulsations and performance characteristics of a centrifugal pump. *Comput. Fluids* **2009**, *38*, 1243–1257. [[CrossRef](#)]
4. Wang, Y.; Zhang, X.; Li, Y.B. Off design flow field analysis and radial force prediction of centrifugal pump. *Drain. Irrig. Mach.* **2008**, *26*, 18–22.
5. Zhang, M.; Tsukamoto, H. Unsteady hydrodynamic forces due to rotor-stator interaction on a diffuser pump with identical number of vanes on the impeller and diffuser. *J. Fluids Eng.* **2005**, *127*, 743–751. [[CrossRef](#)]
6. Agostinelli, A.; Nobles, D.; Mockridge, C.R. An experimental investigation of radial thrust in centrifugal pumps. *ASME J. Eng. Power* **1960**, *82*, 120–125. [[CrossRef](#)]
7. Biheller, H.J. Radial forces on the impeller of centrifugal pumps with volute, semivolute, and fully concentric casings. *ASME J. Eng. Power* **1965**, *87*, 319–323. [[CrossRef](#)]
8. Guelich, J.; Jud, W.; Hughes, S.F. Review of parameters influencing hydraulic forces on centrifugal impellers. *Proc. Inst. Mech. Eng. Part A* **1987**, *201*, 163–174. [[CrossRef](#)]
9. Baun, D.O.; Flack, R.D. A plexiglas research pump with calibrated magnetic bearing/load cells for radial and axial hydraulic force measurements. *ASME J. Fluids Eng.* **1999**, *121*, 126–132. [[CrossRef](#)]
10. Daniel, O.B.; Ronald, D.F. Effects of volute design and number of impeller blades on lateral impeller forces and hydraulic performance. *Int. J. Rotating Mach.* **2003**, *9*, 145–152.
11. Asuaje, M.; Bakir, F.; Kouidri, S.; Kenyery, F.; Rey, R. Numerical modelization of the flow in centrifugal pump: Volute influence in velocity and pressure fields. *Int. J. Rotating Mach.* **2005**, *2005*, 244–255. [[CrossRef](#)]

12. Kang, C.; Li, Y.X. The effect of twin volutes on the flow and radial hydraulic force production in a submersible centrifugal pump. *J. Power Energy* **2015**, *229*, 221–237. [[CrossRef](#)]
13. Khalifa, A.E.; Al-Qutub, A.M.; Ben-Mansour, R. Study of pressure fluctuations and induced vibration at blade-passing frequencies of a double volute pump. *Arabian J. Sci. Eng.* **2011**, *36*, 1333–1345. [[CrossRef](#)]
14. Gonzalez, J.; Fernandez, J.; Blanco, E.; Santolaria, C. Numerical simulation of the dynamic effects due to impeller-volute interaction in a centrifugal pump. *J. Fluids Eng.* **2002**, *124*, 348–355. [[CrossRef](#)]
15. Yang, M.; Min, S.M.; Wang, F.J. Numerical simulation of pressure fluctuation and radial force in a double volute pump. *Trans. Chin. Soc. Agric. Mach.* **2009**, *40*, 83–88.
16. Gonzalez, J.; Parrondo, J.; Santolaria, C.; Blanco, E. Steady and unsteady radial forces for a centrifugal pump with impeller to tongue gap variation. *Trans. ASME* **2006**, *128*, 454–462. [[CrossRef](#)]
17. Liu, J.R.; Fu, D.P.; He, X.K. Optimization design of double-volute splitter in ES250-370 double-suction pump. *Trans. Chin. Soc. Agric. Mach.* **2014**, *45*, 96–100.
18. Liu, J.R.; Xu, Y.G.; Su, Q.Q.; Wang, D.M. Analysis of radial force in centrifugal pump with single and double volute based on FLUENT. *Drain. Irrig. Mach.* **2009**, *27*, 83–86.
19. Guan, X.F. *Modern Pumps Theory and Design*; China Astronautic Publishing House: Beijing, China, 2011.
20. Johann, F.G. *Centrifugal Pumps*; Springer: Berlin/Heidelberg, Germany, 2014.
21. ISO. *ISO 9906 Rotordynamic Pumps—Hydraulic Performance Acceptance Tests—Grades 1 and 2*; International Standardization Organization: Geneva, Switzerland, 1999.
22. Menter, F.R. Review of the shear-stress transport turbulence model experience from an industrial perspective. *Int. J. Comput. Fluid* **2009**, *23*, 305–316. [[CrossRef](#)]



© 2019 by the authors. Licensee MDPI, Basel, Switzerland. This article is an open access article distributed under the terms and conditions of the Creative Commons Attribution (CC BY) license (<http://creativecommons.org/licenses/by/4.0/>).